

# Numerical simulation for solid-liquid phase change of metal sodium in combined wick

Yu Ping<sup>1</sup> Zhang Hong<sup>1,2</sup> Xu Hui<sup>1</sup> Shen Yan<sup>1</sup>

(<sup>1</sup>College of Energy, Nanjing University of Technology, Nanjing 211816, China)

(<sup>2</sup>Changzhou Institute of Technology, Changzhou 213002, China)

**Abstract:** Based on the finite volume method and the enthalpy-porous model, the solid-liquid phase change of sodium in the combined wick is numerically studied. The one-temperature model is used since the thermal conductivity of sodium is close to that of the combined wick materials. The non-Darcy law and natural convection in the melting process are taken into account. The results show that a thin metal fiber felt in the combined wick can result in a faster melting rate of the sodium and a shorter time for the molten sodium to reach the maximum velocity, which can shorten the time for the high-temperature heat pipe startup. A thick metal fiber felt in the combined wick can result in a uniform temperature distribution in the vertical heating wall and a small wall temperature difference, which can reduce the possibility of an overheat spot.

**Key words:** solid-liquid phase change; combined wick; sodium; porous media

**doi:** 10.3969/j.issn.1003-7985.2014.04.010

Metal sodium embedded in the porous media of a heat pipe wick is initially in a solid state before the high-temperature heat pipe startup<sup>[1]</sup>. When power is applied to the evaporator section of the heat pipe, metal sodium in the porous media begins to melt, and natural convection takes place in the molten region because of the density difference of the molten sodium under the gravitational field. The natural convection heat transfer has important effects on the motion speed and shape of the solid/liquid phase change interface, and then further influences the high-temperature heat pipe startup process. Thus, the study on the solid-liquid phase change in porous media has attracted considerable attention<sup>[2-6]</sup>.

Beckermann et al.<sup>[7]</sup> conducted experimental and numerical investigations on the metal gallium phase change in porous media of glass beads. Natural convection was taken into account, and the heat transfer was ignored be-

tween the porous media and the phase change materials on account of the thermal diffusivity being in the same order of magnitude. The numerical results of the solid-liquid phase change interface shape and temperature distribution with a one-temperature model agreed reasonably well with the experimental results. However, if the thermal diffusivity of the porous media exceeds significantly that of the phase change materials, the heat transfer between them should not be ignored. Yang et al.<sup>[8]</sup> used a two-temperature model to simulate numerically solid-liquid phase change in the porous media, accounting for the thermal non-equilibrium between the phase change materials and the metal foam. They found that interstitial heat transfer can enhance the melting process significantly and improve the overall heat transfer rate. Volume expansion of the phase change materials during melting caused an extra flow that suppressed the propagation of the melting front, and consequently decreased the melting rate. Li et al.<sup>[9]</sup> developed a two-equation physical and mathematical model to describe the solid-liquid phase change process in the porous metallic foam. The natural convection of molten paraffin and the local thermal non-equilibrium between the porous metallic foam and the paraffin were taken into account. The study found that under the same pore density of the metallic foam, a smaller porosity, which had a greater effective thermal conductivity, can result in a higher melting rate.

This paper mainly studies the solid-liquid phase change of metal sodium in the porous media of the combined wick of the high-temperature heat pipe<sup>[10-11]</sup>. The combined wick porous media is initially filled with solid sodium, and it melts gradually in the startup process from its frozen state. The melting time of solid sodium and the temperature distribution both have an effect on the high-temperature heat pipe startup process. Therefore, it is necessary to investigate the solid-liquid sodium phase change process in porous media of the combined wick. The solid-liquid sodium phase change process in the combined wick is numerically studied using the finite volume method and enthalpy-porous model. Since the thermal conductivity of the sodium and that of the combined wick (314L stainless steel) are in the same order of magnitudes, one-temperature model is applied<sup>[7,9]</sup> to the current model. The non-Darcy law and the natural convection of

**Received** 2014-05-06.

**Biographies:** Yu Ping (1985—), female, graduate; Zhang Hong (corresponding author), female, doctor, professor, hzhang@njut.edu.cn.

**Foundation items:** The National Natural Science Foundation of China (No. 51076062), the Scientific Innovation Research of College Graduates in Jiangsu Province (No. CXZZ12\_0421).

**Citation:** Yu Ping, Zhang Hong, Xu Hui, et al. Numerical simulation for solid-liquid phase change of metal sodium in combined wick[J]. Journal of Southeast University (English Edition), 2014, 30(4): 456 – 461. [doi: 10.3969/j.issn.1003-7985.2014.04.010]

liquid sodium are also taken into account. Issues investigated and discussed in this paper include the velocity field, the temperature profiles, and the motion rate of the phase change interface.

## 1 Mathematical Formulation and Physical Model

### 1.1 Physical model

In this paper, the combined wick<sup>[11]</sup> is defined as a whole porous media, in which the phase change process of sodium is discussed. The metal fiber felt thickness  $\delta$  in the combined wick has three sizes: 2, 3 and 4 mm. The permeabilities of the combined wick with  $\delta$  of 2, 3 and 4 mm are about  $3.37 \times 10^{-10}$ ,  $2.46 \times 10^{-10}$ , and  $1.05 \times 10^{-10} \text{ m}^2$ , respectively<sup>[11]</sup>.

The physical model used is shown in Fig. 1. The computational domain taken randomly from the combined wick is 100 mm  $\times$  100 mm, which is filled uniformly with the rigid, porous media saturated with the solid sodium. We only simulate the initial state of the high-temperature heat pipe startup from the frozen state, namely the process of the solid sodium melting. In order to simulate the operating conditions of the high-temperature heat pipe, the heat flux boundary condition is used. The heat flux on the wall  $W_1$  is 63 kW/m<sup>2</sup>. The other three faces are adiabatic. Initially, the model was at a uniform temperature of 30 °C.

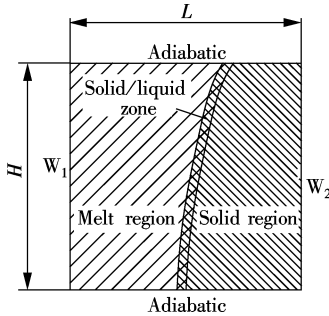


Fig. 1 Schematic illustration of the physical model

### 1.2 Mathematical Model

#### 1.2.1 Assumptions

The following simplifying assumptions are made to obtain the volume averaged conservation equations:

- 1) The flow and heat transfer are two-dimensional and laminar.
- 2) The porous media and fluid are incompressible and the Boussinesq approximation can be invoked.
- 3) The porous media and the sodium (solid or liquid) are at a local thermal equilibrium.

#### 1.2.2 Governing equation

Porous media is modeled by adding a momentum source term to the standard fluid flow equations. The source term is composed of two parts: a viscous loss term and an inertial loss term:

$$S_i = - \left( \frac{\mu_i}{K_i} + \frac{\rho_i C_{fi}}{\sqrt{K_i}} |\mathbf{U}| \right) u_i \quad (1)$$

where  $i$  represents the  $x$  or  $y$  directions;  $S_i$  is the source term;  $\mu_i$  is the dynamic viscosity;  $|\mathbf{U}|$  is the magnitude of the velocity;  $K_i$  is the permeability of the porous media;  $\rho_i$  is the density of fluid and  $C_{fi}$  is the inertial resistance factor. According to Darcy's law<sup>[12]</sup>, in laminar flows through porous media, the viscous loss term in the source term is typically proportional to the velocity, and the inertial resistance factor  $C_{fi}$  can be considered to be zero. According to Darcy-Forchheimer's law<sup>[13–16]</sup>, the inertial resistance factor  $C_{fi}$  in Eq. (1) provides a correction for inertial losses in the porous media in turbulent flows.

According to the above assumptions, the volume averaged conservation equations are

$$\nabla \cdot (\rho_1 \mathbf{U}) = 0 \quad (2)$$

$$\frac{\rho_1}{\delta} \frac{\partial u}{\partial t} + \frac{1}{\delta^2} [\nabla \cdot (\rho_1 \mathbf{U} u)] = - \frac{\partial p}{\partial x} + \frac{\mu_i}{\delta} \nabla^2 u - \left( \frac{\mu_i}{K_x} + \frac{\rho_i C_{fx}}{\sqrt{K_x}} |\mathbf{U}| \right) u \quad (3)$$

$$\frac{\rho_1}{\delta} \frac{\partial v}{\partial t} + \frac{1}{\delta^2} [\nabla \cdot (\rho_1 \mathbf{U} v)] = - \frac{\partial p}{\partial y} + \frac{\mu_i}{\delta} \nabla^2 v - \left( \frac{\mu_i}{K_y} + \frac{\rho_i C_{fy}}{\sqrt{K_y}} |\mathbf{U}| \right) v + \rho_1 g \beta (T - T_{\text{melt}}) \quad (4)$$

$$\frac{\partial}{\partial t} [\varepsilon (\gamma \rho_l h_l + (1 - \gamma) \rho_s h_s) + (1 - \varepsilon) \rho_p h_p] + \nabla \cdot (\rho_1 h_1 \mathbf{U}) = \nabla \cdot (k_{\text{eff}} \nabla T) \quad (5)$$

where  $\mathbf{U}$  is the velocity vector;  $p$  is the pressure;  $\beta$  is the coefficient of thermal expansion; and  $T_{\text{melt}}$  is the melting temperature of the sodium;  $\varepsilon$  is the fraction fluid in the volume element (that is, porosity),  $\varepsilon = V_f/V$ ;  $\gamma$  is the fraction liquid in fluid,  $\gamma(t) = V_l(t)/V_f$ ;  $\delta$  is the fraction liquid in the volume element,  $\delta(t) = V_l(t)/V = \varepsilon \gamma(t)$ .

## 2 Results and Discussion

### 2.1 Model validation

In order to validate the current model, we numerically simulate the experiment in Ref. [7], and then compare the numerical results with the experimental ones at various times. According to the experiment conditions, the temperatures on the hot and cold walls ( $W_1$  and  $W_2$ ) are 45 and 20 °C, respectively, and the other walls are maintained adiabatic. The height and width of the computational domain are both 100 mm, with the porosity of 0.39. The density of the glass spheres is 2343 kg/m<sup>3</sup>; the thermal capacity is 813.56 J/(kg  $\cdot$  K) and the thermal conductivity is 0.79 W/(m  $\cdot$  K). The melting point

of gallium is 302.93 K; the density is 6 095 kg/m<sup>3</sup>; the thermal capacity is 397.91 J/(kg · K); the latent heat of melting is 80.16 kJ/kg; the thermal conductivity is 17.39 to 29.26 W/(m · K); and the coefficient of thermal expansion is  $6.31 \times 10^{-5}$  1/K. The  $x$  and  $y$  coordinates and the temperature  $T$  are all transformed into dimensionless parameters in order to compare and observe them easily; namely,  $X = \frac{x}{H}$ ,  $Y = \frac{y}{H}$ ,  $\theta_i = \frac{T_i - T_{w1}}{T_{w2} - T_{w1}}$ .

Figs. 2 and 3 show the comparisons of the evolution of the melting front and temperature profiles between the present model and the experimental results in Ref. [7]. From Fig. 2 ( $t = 1$  to 5 min) and Fig. 3 (a), the deviation between the numerical simulation results and experimental ones in the early melting process is due to the uneven packing of the glass beads at the top of the computational domain. The loose packing causes the local volume fraction of gallium to be larger near the top than in the lower layers, which requires a larger amount of heat to melt them and can explain the slower advance of the melting front. Later in the process ( $t = 20$  min), the melting rate of gallium is greatly reduced due to the lower temperature gradients. As the melting rate decreases, the heat transfer is dominated by conduction and convection, and the effect of the uneven packing of glass beads (volume fraction of gallium) on the temperature profile and melting front is greatly diminished. Under these conditions, a good agreement is observed between the measured and predicted melting front locations and temperature profiles, as shown in Fig. 2 ( $t = 20$  min) and Fig. 3 (b).

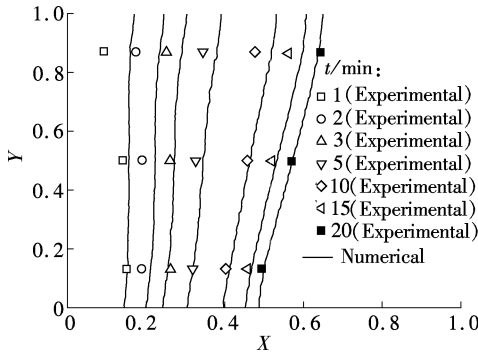


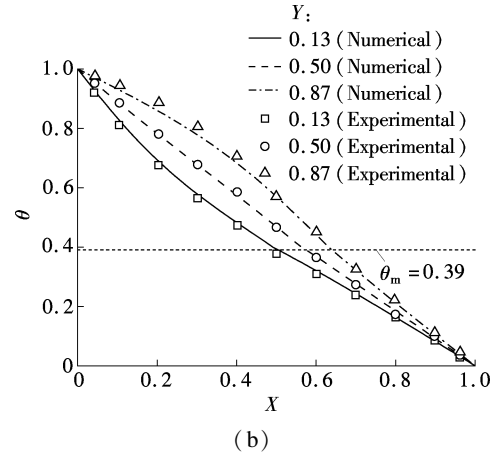
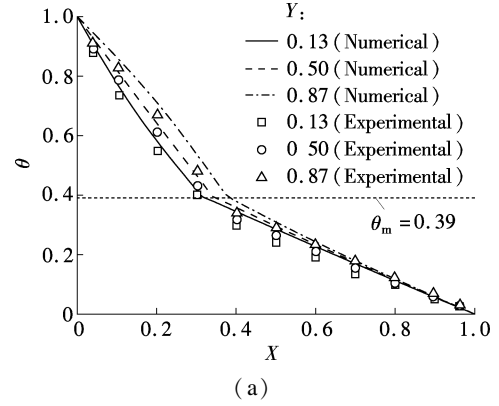
**Fig. 2** Comparison of the evolution of the melting front

From the above analysis, the current model is valid and can be applied to study a sodium melting process in the porous media of the combined wick.

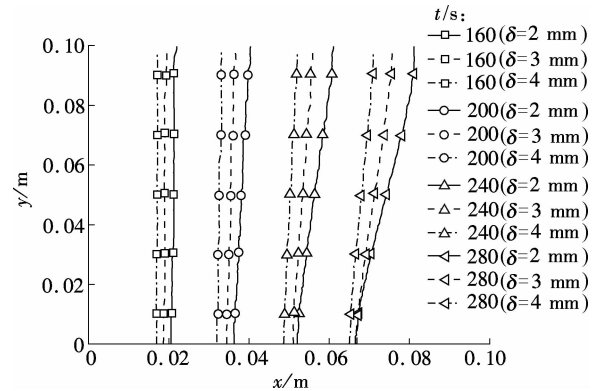
## 2.2 Relationship between the structure and the motion speed of the melting front

Fig. 4 illustrates the evolution of the melting front in the combined wick with different  $\delta$ . In the initial stage of melting, the melting front of sodium moves from the left wall to the right wall gradually. It can be seen that a thinner  $\delta$  results in a higher melting rate in the combined wick. The reason is, on the one hand, that the flow re-

distance becomes less in the combined wick when a thinner  $\delta$  results in a larger permeability. On the other hand, the porosity of the combined wick is less when  $\delta$  is thinner. Less porosity means less solid sodium embedded in the combined wick; thus the absorbed heat is less under the melting process of sodium. The motion speed of the melting front is faster.



**Fig. 3** Comparison of experimental results in Ref. [7] and numerical results from proposed model. (a)  $t = 5$  min; (b)  $t = 20$  min



**Fig. 4** Comparison of the evolution of the melting front in the combined wick with different  $\delta$

Due to the above reasons, the sodium will have a higher melting rate in the combined wick with a thinner  $\delta$ , and the heat transfer rate is also higher and then the time for the high-temperature heat pipe startup becomes shorter.

ter. It is very important when requiring a fast startup.

### 2.3 Distribution of temperature and velocity

In the process of the sodium melting, the temperature profiles and the distribution of fluid flow in the combined wick with  $\delta$  of 2, 3 or 4 mm are similar, and thus we only discuss the phase change process in the combined wick with  $\delta$  of 2 mm in this paper.

Fig. 5 shows the temperature profiles of three different vertical sections in the combined wick with  $\delta$  of 2 mm of 180 and 220 s, respectively. The melting point of sodium is about 370.97 K. The corresponding predicted streamlines are shown in Fig. 6.

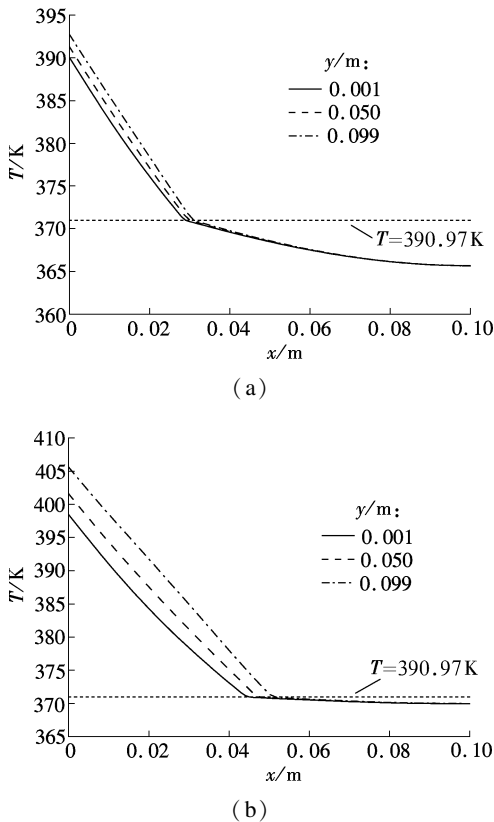


**Fig. 5** Temperature profiles of three different vertical sections in the combined wick with  $\delta$  of 2 mm. (a)  $t = 180$  s; (b)  $t = 220$  s

From Figs. 5(a) and (b), it can be seen that the temperature difference between the top of the model ( $y = 0.099$  m) and the bottom of the model ( $y = 0.001$  m) becomes larger and larger with the melting process. The reason is that the sodium close to the heating wall melts first in the initial period; the melting front is almost parallel to the heating wall indicating a conduction dominated melting process; thus the temperature difference at the heating wall is very small, as shown in Fig. 6(a). After the initial period, with the amount of molten sodium increasing continuously, buoyancy induced convection heat transfer in the melting becomes increasingly significant, and the melting front gradually becomes the typical shape of convection dominated melting, as shown in Fig. 6(b). The melting front moves faster near the top where the liq-

uid, heated by the hot wall, flows in constantly. However, the melting rate decreases toward the bottom, because the liquid cools as it descends along the interface.

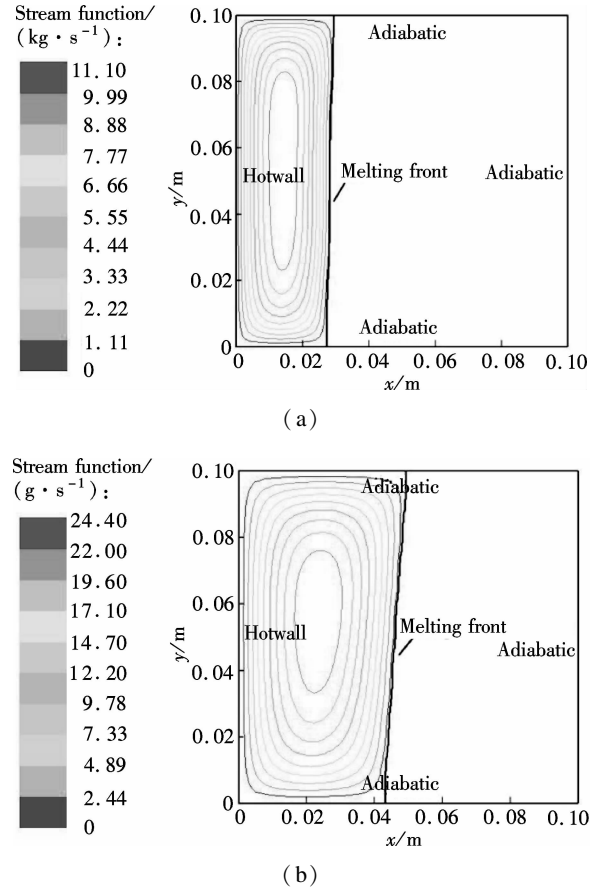


**Fig. 6** Velocity fields in the combined wick with  $\delta$  of 2 mm. (a)  $t = 180$  s; (b)  $t = 220$  s

### 2.4 Effect of the wick structure on the temperature distribution

Fig. 7 shows the temperature distribution of the heating wall with different  $y$ -coordinates in the combined wick with different  $\delta$  in the sodium melting period. It can be seen that with the melting process, the heating wall temperature difference becomes larger and larger. In the initial period, the temperature distribution on the heating wall is uniform, thus the temperatures at different  $y$ -coordinates are almost the same, as shown in Fig. 7 ( $t = 0$  to 180 s). With the amount of molten sodium increasing, the convection induced by the density difference becomes more and more significant. The hot upward flow of liquid sodium results in a higher melting rate in the upper region, so the non-uniform temperature distribution on the heating wall appears. As shown in Fig. 7, the temperature differences between  $y = 0.001$  m and  $y = 0.099$  m in the heating wall of the combined wick are about 14.10, 8.83 and 6.07 K corresponding to  $\delta$  of 2, 3 and 4 mm, respectively, for  $t = 280$  s. It is observed that a thicker  $\delta$  in the combined wick can lead to a more uniform temperature

distribution in the vertical heating wall, and a smaller temperature difference. In most cases, when the temperature distribution in the heating wall is uneven, the overheat spot will likely appear and the process of the high-temperature heat pipe startup may fail. Therefore, a thicker  $\delta$  is beneficial.

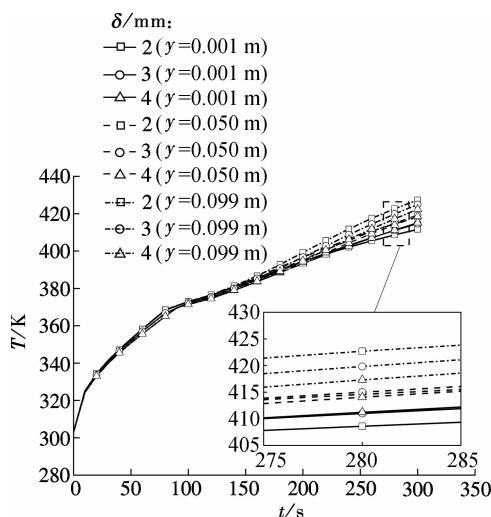


Fig. 7 The variation of the temperature distribution in the heating wall  $W_1$

## 2.5 Relationship between structure of the combined wick and melting rate

Fig. 8 shows the variation of the maximum velocity of molten sodium in the process of sodium melting in the combined wick with different  $\delta$ . It can be seen that in the process of sodium melting there are three obvious stages for the maximum velocity variation, namely, appearance, increasing and decreasing. The maximum velocity of molten sodium increases first, reaches the peak value and then decreases. The peak values in the combined wick with  $\delta$  of 2, 3 and 4 mm are about 0.002 55, 0.001 68 and 0.001 26 m/s, respectively, and the corresponding times are 320, 340 and 350 s, respectively. The reason is, first, that a thicker  $\delta$  in the combined wick will result in a higher flow resistance, and thus the maximum

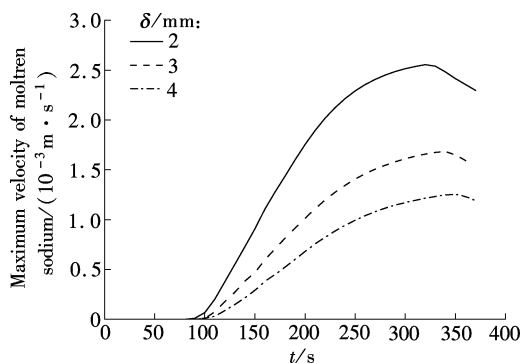


Fig. 8 Variation of the maximum velocity of molten sodium in the process of sodium melting in the combined wick with different  $\delta$

velocity in the melting process of sodium is smaller. Secondly, the porosity of the combined wick is larger when  $\delta$  is thicker, and the amount of solid sodium embedded in the combined wick is larger, and thus the amount of absorbed heat is larger under the melting process of sodium.

From the above, the heat transfer capability of the combined wick will weaken with thickening the metal fiber felt, and the maximum velocity of molten sodium will take more time to reach its peak value.

## 3 Conclusions

1) With a thinner  $\delta$ , the melting rate is higher, and it will take less time for the molten sodium to reach the maximum velocity.

2) Due to the natural convection, the hot upward flow of the liquid sodium results in a higher melting rate and temperature in the upper region of the combined wick than those of the bottom.

3) The temperature distribution in the vertical heating wall  $W_1$  is more uniform in the thicker metal fiber felt of the combined wick.

In conclusion, if the melting rate of sodium in the combined wick with a thinner  $\delta$  is high, then the time of the high-temperature heat pipe startup can be shortened. However, a thinner  $\delta$  will result in a more nonuniform temperature distribution of the heating wall, which increases the possibility of an overheat spot and influences the property of the high-temperature heat pipe. As a result, in the design process of high-temperature heat pipes, the above factors need to be considered fully.

## References

- [1] Zhuang Jun, Zhang Hong. *Heat pipe technology and engineering application* [M]. Beijing: Chemical Industry Press, 2000: 66–67. (in Chinese)
- [2] Jones B J, Sun D, Krishnan S, et al. Experimental and numerical study of melting in a cylinder[J]. *International Journal of Heat and Mass Transfer*, 2006, **49** (15/16): 2724–2738.
- [3] Zhang Yanchen, Gao Dongyan, Chen Zhenqian. Influence of porosity on melting of phase change materials in metal foams with lattice Boltzmann method[J]. *Journal of Southeast University: Natural Science Edition*, 2013, **43** (1): 94–98. (in Chinese)
- [4] Jany P, Bejan A. Scaling theory of melting with natural convection in an enclosure[J]. *International Journal of Heat and Mass Transfer*, 1988, **31** (6): 1221–1235.
- [5] Sun D, Garimella S V, Singh S, et al. Numerical and experimental investigation of the melt casting of explosives[J]. *Propellants, Explosives, Pyrotechnics*, 2005, **30** (5): 369–380.
- [6] Krishnan S, Murthy J Y, Garimella S V. A two-temperature model for solid-liquid phase change in metal foams [J]. *Journal of Heat Transfer*, 2005, **127** (9): 995–1004.
- [7] Beckermann C, Viskanta R. Natural convection solid/liq-

- uid phase change in porous media [J]. *International Journal of Heat and Mass Transfer*, 1988, **31**(1): 35 – 46.
- [8] Yang Z, Garimella S V. Melting of phase change materials with volume change in metal foams[J]. *Journal of Heat Transfer*, 2010, **132**(6): 062301-1 – 062301-11.
- [9] Li Wenqiang, Qu Zhiguo, Tao Wenquan. Numerical study of solid-liquid phase change in metallic foam[J]. *Journal of Engineering Thermophysics*, 2013, **34**(1): 141 – 144. (in Chinese)
- [10] Bai Tong, Zhang Hong, Xu Hui, et al. Performance study on a novel combined wick of heat pipe[J]. *Proceedings of the CSEE*, 2011, **31**(23): 79 – 85. (in Chinese)
- [11] Bai Tong, Zhang Hong, Xu Hui, et al. Investigations of flow resistance through combined heat pipe wick [J]. *Journal of Nanjing University of technology: Natural Science Edition*, 2012, **34**(1): 56 – 60. (in Chinese)
- [12] Gray W G, O'neill K. On the general equations for flow in porous media and their reduction to Darcy's law[J]. *Water Resources Research*, 1976, **12**(2): 148 – 154.
- [13] Vafai K, Tien C L. Boundary and inertia effects on flow and heat transfer in porous media[J]. *International Journal of Heat and Mass Transfer*, 1981, **24**(2): 195 – 203.
- [14] Liu J F, Wu W T, Chiu W C, et al. Measurement and correlation of friction characteristic of flow through foam matrixes[J]. *Experimental Thermal and Fluid Science*, 2006, **30**(4): 329 – 336.
- [15] Wu W T, Liu J F, Li W J, et al. Measurement and correlation of hydraulic resistance of flow through woven metal screens [J]. *International Journal of Heat and Mass Transfer*, 2005, **48**(14): 3008 – 3017.
- [16] Beavers G S, Sparrow E M, Rodenz D E. Influence of bed size on the flow characteristics and porosity of randomly packed beds of spheres [J]. *Journal of Applied Mechanics*, 1973, **40**(3): 655 – 660.

## 组合式吸液芯内金属钠固-液相变的数值模拟

于 萍<sup>1</sup> 张 红<sup>1,2</sup> 许 辉<sup>1</sup> 沈 妍<sup>1</sup>

(<sup>1</sup> 南京工业大学能源学院, 南京 211816)

(<sup>2</sup> 常州工学院, 常州 213002)

**摘要:**采用有限容积法和焓-多孔介质模型数值模拟了组合式吸液芯内金属钠熔化的固-液相变过程. 由于液态金属钠和组合式吸液芯的导热系数在同一数量级, 因而采用单温度模型, 模拟过程中考虑了非达西效应影响和液态金属钠的自然对流现象. 研究结果发现, 组合式吸液芯中金属纤维毡厚度越小, 金属钠受热熔化的速度越快, 且熔化后的液态钠流速达到最大值所用的时间越短, 进而可以缩短热管启动时间; 组合式吸液芯中金属纤维毡厚度越大, 竖直加热壁面的温度分布越均匀、壁面温差越小, 进而减少了加热壁面产生过热点的可能.

**关键词:**固-液相变; 组合式吸液芯; 金属钠; 多孔介质

**中图分类号:**TK172.4